



Published in final edited form as:

*Nat Neurosci.* 2013 May ; 16(5): 613–621. doi:10.1038/nn.3356.

## Physiological Brain Activity Causes DNA Double Strand Breaks in Neurons — Exacerbation by Amyloid- $\beta$

Elsa Suberbielle<sup>1,2</sup>, Pascal E. Sanchez<sup>1,2</sup>, Alexxai V. Kravitz<sup>1,2</sup>, Xin Wang<sup>1</sup>, Kaitlyn Ho<sup>1</sup>, Kirsten Eilertson<sup>3</sup>, Nino Devidze<sup>1</sup>, Anatol C. Kreitzer<sup>1,2</sup>, and Lennart Mucke<sup>1,2</sup>

<sup>1</sup>Gladstone Institute of Neurological Disease, San Francisco, California 94158

<sup>2</sup>Department of Neurology, University of California, San Francisco, San Francisco, California 94158

<sup>3</sup>Gladstone Institute of Cardiovascular Disease, San Francisco, California 94158

### Abstract

We show that a natural behavior, exploration of a novel environment, causes DNA double-strand breaks (DSBs) in neurons of young adult wildtype mice. DSBs occurred in multiple brain regions, were most abundant in the dentate gyrus, which is involved in spatial learning and memory, and were repaired within 24 hours. Increasing neuronal activity by sensory or optogenetic stimulation increased neuronal DSBs in relevant but not irrelevant networks. Human amyloid precursor protein (hAPP) transgenic mice, which simulate key aspects of Alzheimer's disease, had increased neuronal DSBs at baseline and more severe and prolonged DSBs after exploration. Interventions that suppress aberrant neuronal activity and improve memory in hAPP mice normalized their levels of DSBs. Blocking extrasynaptic NMDA-type glutamate receptors prevented amyloid- $\beta$  (A $\beta$ )-induced DSBs in neuronal cultures. Thus, transient increases in neuronal DSBs occur as a result of physiological brain activity and A $\beta$  exacerbates DNA damage, most likely by eliciting synaptic dysfunction.

### INTRODUCTION

Neuronal DNA damage may contribute to cognitive aging and the pathogenesis of neurodegenerative disorders such as Alzheimer disease (AD)<sup>1,2</sup>. Aging, the main risk factor for these disorders, is associated with a progressive increase in markers of DNA breaks in neurons<sup>3</sup>. One such marker is phosphorylation of the histone protein H2A variant X at serine 139 (resulting in  $\gamma$ H2A.X), which reliably identifies DNA double-strand breaks (DSBs)<sup>4,5</sup>.

Users may view, print, copy, download and text and data- mine the content in such documents, for the purposes of academic research, subject always to the full Conditions of use: [http://www.nature.com/authors/editorial\\_policies/license.html#terms](http://www.nature.com/authors/editorial_policies/license.html#terms)

**Address for correspondence** Lennart Mucke, MD Gladstone Institute of Neurological Disease 1650 Owens Street San Francisco, CA 94158 Tel.: 415-734-2504 Fax: 415-355-0131 [lmucke@gladstone.ucsf.edu](mailto:lmucke@gladstone.ucsf.edu).

#### Author Contributions

E.S. designed and conducted behavioral, immunohistochemical and biochemical analyses. P.E.S. designed and carried out levetiracetam treatments and stress-related studies. A.V.K. designed and conducted optogenetic experiments. X.W. and K.H. provided technical assistance for biochemical analyses. K.E. contributed to statistical analyses. N.D. helped design behavioral paradigms. A.C.K. supervised the optogenetic experiments. E.S. and L.M. analyzed and interpreted data and wrote the manuscript. L.M. conceived of, supervised and provided funding for the study.

Many studies of  $\gamma$ H2A.X have focused on the relationship between severe DNA damage and the activation of cell death pathways<sup>1, 4-6</sup>. However,  $\gamma$ H2A.X may also help recruit the DNA repair machinery and fulfill physiological functions in epigenetic processes that regulate chromatin structure and gene expression. For example,  $\gamma$ H2A.X appears to be involved in mitosis, meiosis, lymphocyte development, neural development and adult neurogenesis<sup>7-10</sup>. In proliferating cells, its activation is typically associated with a pause in cell cycle progression<sup>4</sup>. In cultures of differentiated neurons,  $\gamma$ H2A.X levels increased transiently after stimulation with NMDA<sup>11</sup>, suggesting a potential link between neuronal activity and DSBs. Activation of  $\gamma$ H2A.X has been identified as a predictor of neuronal death and an early marker of nonlethal neuronal harm caused by kainate-induced epileptic activity<sup>12</sup> in rats.

Here, we used  $\gamma$ H2A.X measurements and related approaches to examine the causes, extent and duration of neuronal DSBs in the brains of mice under physiological and pathophysiological circumstances. Physiological stimulation was achieved by allowing mice to explore a novel environment, which causes widespread, transient neuronal activation<sup>13, 14</sup>. This natural behavior, visual stimulation in anesthetized mice, and optogenetic activation of striatal neurons in awake behaving mice each caused significant increases in neuronal DSBs in specific brain regions of wildtype mice. We also investigated DSBs in human amyloid precursor protein (hAPP) transgenic mice from line J20 (hAPP mice). These mice exhibit several features of AD, including pathologically elevated levels of amyloid- $\beta$  (A $\beta$ ) peptides in the brain, age-dependent deficits in learning and memory, behavioral abnormalities, synaptic deficits, aberrant neuronal network activity, formation of neuritic amyloid plaques, and inflammatory reactions of astrocytes and microglia<sup>15-19</sup>. Virtually all of these phenotypes have also been identified in other lines of hAPP transgenic mice<sup>18, 20-22</sup>. Compared to wildtype controls, hAPP mice had a larger number of neurons with DSBs at baseline as well as greater and more prolonged increases in DSBs after exploration of a novel environment. Suppression of aberrant network activity in hAPP mice prevented and reversed the baseline increase in neuronal DSBs. Consistent with these *in vivo* findings, A $\beta$  oligomers caused DSBs to form in primary neuronal cultures, and this effect could be prevented by blocking extrasynaptic NMDA-type glutamate receptors (NMDARs). We conclude that transient increases in neuronal DSBs are an integral component of physiological brain activity and that A $\beta$  exacerbates DNA damage by eliciting aberrant synaptic activity.

## RESULTS

### Pathological levels of A $\beta$ increase neuronal $\gamma$ H2A.X

To determine whether pathologically elevated levels of A $\beta$  cause neuronal DNA damage, we counted cells that had at least one  $\gamma$ H2A.X-immunoreactive focus in the nucleus (Fig. 1a) in several brain regions of hAPP-J20 transgenic and wildtype mice at 6 months of age, when hAPP mice from this line have cognitive deficits and their brains contain pathogenic soluble A $\beta$  assemblies but few amyloid deposits<sup>15, 16</sup>. In all brain regions studied, hAPP mice had 2.0–3.5 times more  $\gamma$ H2A.X-positive cells than wildtype controls (Fig. 1b). The  $\gamma$ H2A.X foci were located primarily in neurons, as shown by co-labeling of brain sections for NeuN (Fig. 1a). Even at 1.0–1.5 months of age, before hAPP mice show behavioral abnormalities,

the number of  $\gamma$ H2A.X-positive cells in the hippocampus and neocortex was higher in hAPP than wildtype mice (Fig. S1), indicating that this alteration precedes—and thus might contribute to—the development of cognitive decline.

In addition to increased levels of A $\beta$ , hAPP mice also have increased levels of other hAPP metabolites in the brain. We therefore determined whether A $\beta$  oligomers were sufficient to increase neuronal  $\gamma$ H2A.X formation in cultured primary neurons from wildtype mice. Adding A $\beta$  oligomers to the cultures increased  $\gamma$ H2A.X levels threefold (Fig. 1c).

### Exploratory behavior increases neuronal $\gamma$ H2A.X foci in mice

In the course of our experiments, we made the intriguing observation that exploration of a novel environment increased the number of neurons with  $\gamma$ H2A.X foci in wildtype mice. This behavioral paradigm is well known to increase neuronal activity in multiple brain regions, as reflected by widespread increases in neuronal expression of the activity-regulated cytoskeletal protein Arc<sup>13, 14</sup>. Wildtype mice that explored the novel environment had more  $\gamma$ H2A.X-positive neurons in different brain regions, particularly in the dentate gyrus, than controls that remained in their home cages (Figs. 2a,b and S2a–c). Exploration also increased dentate levels of Spo11 (Fig. S2d–e), an endonuclease known to cause physiological DSBs during meiosis in the testis<sup>23</sup>. In the mice that explored the novel environment, the number of  $\gamma$ H2A.X-positive neurons returned to baseline levels after a 24-hour recovery period in their home cage (Figs. 2a,b and S2a–c).

As expected, hAPP mice had more  $\gamma$ H2A.X-positive neurons than wildtype mice under control (home cage) conditions (Figs. 2c and S2a–c). Like wildtype controls, hAPP mice showed an increase in  $\gamma$ H2A.X-positive neurons after exploring the novel environment, particularly in the parietal cortex and dentate gyrus (Figs. 2c and S2a–c). Student's t-test revealed no significant differences in the number of  $\gamma$ H2A.X-positive neurons between hAPP and wildtype mice after exploration (Fig. 2b, c). However, because of their increased DNA damage at baseline, the relative fold increase in  $\gamma$ H2A.X-positive neurons after exploration tended to be lower in hAPP than wildtype mice (Figs. 2b,c and S2a–c). Like wildtype mice, hAPP mice had fewer  $\gamma$ H2A.X-positive neurons after a 24-hour recovery than immediately after the novel environment exploration (Figs. 2b,c and S2a–c). However, in the dentate gyrus and parietal cortex of hAPP mice, the decline was less complete than in wildtype mice and did not reach baseline levels (Figs. 2c and S2a–c).

### A $\beta$ - and exploration-induced neuronal DSBs

Although  $\gamma$ H2A.X is a well established marker of DSBs<sup>4, 5, 24</sup>, the notion that a natural behavior would increase neuronal DSBs in wildtype mice was perplexing and required further validation. We therefore immunostained brain sections for 53BP1, another widely accepted marker of DSBs<sup>25, 26</sup>. Roughly 85% percent of  $\gamma$ H2A.X foci were co-labeled for 53BP1, while all 53BP1 foci were also positive for  $\gamma$ H2A.X (Figs. 1d, S3a–c, and data not shown). Because the formation of 53BP1 foci depends on and follows the formation of  $\gamma$ H2A.X foci<sup>26</sup>, it is possible that the small proportion of  $\gamma$ H2A.X foci that did not co-stain for 53BP1 identifies the most recently formed DSBs. The majority of  $\gamma$ H2A.X/53BP1-positive nuclei in the dentate gyrus contained a single focus and 1% or fewer  $\gamma$ H2A.X/

53BP1-positive nuclei had 3 or more foci (Fig. S3d, e). These foci were similar in size and shape to neuronal  $\gamma$ H2A.X foci caused by sublethal doses of whole-body  $\gamma$ -irradiation, which was used as a positive control (Figs. S3a and S4a).

To further assess whether these foci represent DSBs, we analyzed dentate gyrus homogenates by single cell gel electrophoresis (“comet assay”) (Fig. 3). Because fragmented, but not intact, DNA can be electrophoresed out of the nucleus, nuclei containing fragmented DNA show a comet tail in this assay, whose length reflects the extent of DNA damage (Fig. 3a–c). At alkaline pH, the assay detects both single-strand breaks (SSBs) and DSBs, whereas at neutral pH (as used here), the assay is more specific for DSBs<sup>27</sup>. The comet assay confirmed that hAPP mice have an increased number of cells with DSBs at baseline, and that exploration of a novel environment increased the number of cells with DSBs in wildtype mice (Fig. 3d). It also allowed us to quantitate the extent of DNA damage in greater detail.

After exploration of a novel environment, roughly 30–40% of nuclei had comet tails in both hAPP and wildtype mice (Fig. 3d), but the extent of DNA damage was larger in the hAPP mice, as reflected by longer tails and a greater proportion of nuclear DNA that migrated into the tail (Fig. 3e–g). Independent of genotype and behavioral condition, the majority of comet-bearing nuclei had less than 20% of their DNA in the tail (Fig. 3f) and only 10–15% of them had more than 40% of DNA in the tail (Fig. 3g). This extent of DNA damage was comparable to that induced by the lowest dose of whole-body  $\gamma$ -irradiation used here (Fig. S4b, c).

Taken together, these findings strongly support the conclusion that the neuronal  $\gamma$ H2A.X foci we identified in hAPP and wildtype mice represent actual DSBs.

### Neuronal activity, but not stress hormones, causes DSBs

To address the mechanisms by which exploration of a novel environment increases neuronal DSBs, we first focused on stress and corticosterone, the latter of which can increase DNA damage *in vitro*<sup>28</sup>. Compared with the home cage condition, plasma corticosterone levels of wildtype mice were increased after the first 15 min of exploring a novel environment, albeit not as much as after 15 min of restraint stress (Fig. S5a). To determine whether the increase in neuronal DSBs after exploration of a novel environment is caused by increases in the levels of corticosterone or other factors released from the adrenal gland in response to stress, wildtype mice were sham-operated or adrenalectomized (ADX). The latter group was implanted with subcutaneous corticosterone pellets to hold their corticosterone levels constant at physiological baseline levels. Sham-operated, but not ADX, mice showed the expected increases in corticosterone levels after exploring a novel environment for 2 h (Fig. S5b) or being subjected to restraint stress for 15 min (data not shown). However, both groups of mice showed a comparable increase in neurons with DSBs in the dentate gyrus and CA regions of the hippocampus after exploring the novel environment, as compared to mice kept in their home cages (Fig. S5c, d). Thus, exploration-induced increases in DSBs are not caused by stress-induced surges in corticosterone or other adrenal factors.

We then wondered whether increases in neuronal activity might be sufficient to cause DSBs. To test this hypothesis, we employed two experimental paradigms: activation of the primary visual cortex (V1) by exposing anesthetized mice to visual stimuli and activation of the striatum in awake-behaving mice by optogenetic stimulation. In the first paradigm, one eye was exposed to visual stimuli for 15 min, while the other was shielded from light (Fig. 4a). One hour after the visual stimulation began, the number of cells with  $\gamma$ H2A.X foci in the stimulated contralateral V1 was roughly twice as high as that in the unstimulated ipsilateral V1 (Fig. 4b). The number of c-Fos-expressing neurons was used as a positive control and increased to a similar extent in the contralateral V1 (Fig. 4b). The whisker-barrel cortex served as a stimulus-irrelevant negative control and showed no difference in the number of cells with  $\gamma$ H2A.X foci between hemispheres (Fig. 4c).

To optogenetically modulate neuronal activity in the striatum, transgenic A2A-Cre mice, which express Cre-recombinase in the medium spiny projection neurons of the indirect pathway in the dorsomedial striatum, received unilateral striatal injections of adeno-associated virus expressing double-floxed inverted constructs encoding a channelrhodopsin-2(ChR2)-YFP fusion protein or YFP alone. When the transduced striatum was stimulated with light through an implanted optical fiber, ChR2-YFP mice displayed many more ipsiversive rotations than YFP-expressing controls (Fig. 4e). Consistent with this behavioral evidence for indirect pathway activation, illuminated ChR2-YFP-expressing striata contained many more cells with  $\gamma$ H2A.X foci than non-illuminated contralateral striata or illuminated striata expressing only YFP (Fig. 4f). Thus, activation of neuronal activity in specific neuronal networks causes an increase in neuronal DSBs selectively within these networks, but not globally.

### Preventing Aberrant Activity in hAPP Mice Reduces DSBs

hAPP-J20 mice and other lines of hAPP mice show aberrant network activity, including epileptiform spikes and non-convulsive seizures<sup>18, 29-31</sup>, which may relate to the increased incidence of seizures in humans with AD<sup>32</sup>. In hAPP-J20 mice, such aberrant activity can be detected by 6 weeks of age (data not shown), suggesting that it might contribute causally to other abnormalities that become manifest around the same time or thereafter. Consistent with this notion, interventions that prevent or suppress this network dysfunction, such as genetic reduction of tau or treatment with the anti-epileptic drug levetiracetam, improve both synaptic and cognitive functions in hAPP mice<sup>19, 30, 33, 34</sup>. To determine whether tau reduction prevents A $\beta$  from causing neuronal DSBs, we crossed hAPP mice onto a *Tau* knockout (*Tau*<sup>-/-</sup>) background as described<sup>19</sup>, and compared the numbers of neurons with  $\gamma$ H2A.X foci in different brain regions of mice that did or did not express tau and that were exposed to the behavioral conditions summarized in Fig. 2a.

In mice without hAPP expression, tau ablation did not significantly change the number of  $\gamma$ H2A.X-positive neurons at baseline or after recovery compared to wildtype mice (Figs. 2b, 2d, 5a, S2a and S2c). In hAPP mice, tau ablation normalized the number of  $\gamma$ H2A.X-positive neurons in all brain regions to levels found in wildtype mice, both at baseline and after recovery (Figs. 2e, 5a, S2a and S2c). In hAPP mice, tau ablation also brought the fold increase in  $\gamma$ H2A.X-positive neurons in the dentate gyrus immediately after exploration

closer to that seen in wildtype controls (Fig. S2b). A similar trend was observed in hippocampal CA regions (Fig. S2b). The presence of A $\beta$  oligomers increased  $\gamma$ H2A.X levels in primary neuronal cultures from *Tau*<sup>+/+</sup> mice, but not in those from *Tau*<sup>+/-</sup> or *Tau*<sup>-/-</sup> mice (Fig. 5b). Thus, even partial tau reduction prevented A $\beta$  from increasing DSBs in neurons, consistent with the beneficial effects of partial tau reduction on other A $\beta$ -dependent abnormalities, including epileptiform activity, premature mortality, cognitive deficits, and impairments in axonal transport<sup>19, 30, 33</sup>.

Since tau reduction prevents aberrant network activity in different lines of hAPP transgenic mice<sup>33</sup>, the above findings support the hypothesis that the increased levels of neuronal DSBs in hAPP mice are caused by such activity. To test this hypothesis more directly, we treated 4–5-month-old mice with the anti-epileptic drug levetiracetam, which partially suppresses aberrant network activity, reverses synaptic deficits and ameliorates cognitive deficits in hAPP mice<sup>34</sup>. One month of continuous subcutaneous infusion of levetiracetam (75 mg/kg/day) normalized the numbers of  $\gamma$ H2A.X-positive foci in the dentate gyrus and hippocampus of hAPP mice, but had no effect on  $\gamma$ H2A.X-positive foci in wildtype mice (Fig. 6a, b). Treated hAPP mice also showed a trend toward lower numbers of  $\gamma$ H2A.X-positive foci in the entorhinal cortex (Fig. 6c).

### Role of Extrasynaptic NMDARs in Formation of Neuronal DSBs

In cultures of primary wildtype neurons, addition of A $\beta$  oligomers increased the number of  $\gamma$ H2A.X-positive cells and  $\gamma$ H2A.X levels but not in neurons whose activity was reduced with a sodium channel blocker (TTX) or with antagonists of AMPA-type (NBQX) or NMDA-type (APV) glutamate receptors (NMDARs) (Fig. 7a, b). The finding that TTX blocked A $\beta$ -induced increases in DSBs suggests that this A $\beta$  effect depends on action potential-induced synaptic release of neurotransmitters. The finding that NBQX blocked the A $\beta$  effect suggests that postsynaptic depolarization mediated by AMPA receptors is required for this effect. Postsynaptic depolarization is required for removal of the Mg<sup>2+</sup> block of NMDA receptors, which in turn is required for activation of these receptors. The finding that APV blocked the A $\beta$  effect indicates that it indeed depends on activation of NMDA receptors.

Much evidence suggests that the functional consequences of glutamatergic neurotransmission critically depend on the balance between intra- versus extrasynaptic NMDA receptor activation<sup>18, 35</sup>. To determine whether the A $\beta$ -induced enhancement of DSBs requires activation of intrasynaptic or extrasynaptic NMDARs, we cultured neurons under conditions that favor the stimulation of one or the other (Fig. 8a). In the absence of A $\beta$  oligomers,  $\gamma$ H2A.X levels were higher under “extrasynaptic” conditions, whereas levels of phosphorylated ERK1/2 were higher under “intrasynaptic” conditions (Figs. 8b–8d and S6a). Extrasynaptic conditions were also associated with increased production of reactive oxygen species (ROS), but prevention of this increase by pretreatment of cultures with the ROS scavenger Euk-134 did not diminish the increased level of  $\gamma$ H2A.X (Fig. S7).

A $\beta$  oligomers increased  $\gamma$ H2A.X levels more markedly under extrasynaptic conditions (Fig. 8c, d), and the increase was prevented by ifenprodil (Fig. 8c, d), a drug that specifically blocks NR2B-containing NMDARs, which primarily reside extrasynaptically<sup>36</sup>. A $\beta$

oligomers caused more intense  $\gamma$ H2A.X immunoreactivity in neuronal nuclei under extrasynaptic than under control conditions (Fig. 8e, f). Thus, A $\beta$ -induced formation of neuronal DSBs requires action potential-dependent synaptic release of neurotransmitters (TTX), postsynaptic depolarization (NBQX), and activation of NR2B-containing (ifenprodil) NMDARs (APV). Blocking any of these critical elements with the inhibitors indicated in parentheses disrupted the causal chain that connects A $\beta$  to neuronal DNA damage and  $\gamma$ H2A.X formation.

## DISCUSSION

Our study shows that exploratory activity, which is associated with physiological increases in neuronal activity and the encoding of new information, causes widespread increases in neuronal DSBs. DNA damage in post-mitotic cells has previously been demonstrated in pathological contexts<sup>1, 37</sup>. However, to our knowledge, this is the first *in vivo* demonstration of physiologically induced DSBs in post-mitotic cells. Four lines of evidence support the presence of DSBs: (1) the formation of distinct nuclear foci immunoreactive for  $\gamma$ H2A.X, a well established marker of DSBs<sup>4, 5</sup>, (2) the co-labeling of  $\gamma$ H2A.X foci with 53BP1, another widely accepted marker of DSBs<sup>25, 26</sup>, (3) the close resemblance of the foci with foci elicited by doses of  $\gamma$ -irradiation known to cause DSBs<sup>38, 39</sup>, and (4) the detection of DNA fragmentation in single cells by comet assay carried out at neutral pH<sup>27</sup>.

Pathologically elevated levels of A $\beta$  increased neuronal DSBs at baseline and augmented and prolonged the increases in DSBs that resulted from physiological increases in neuronal activity. It is tempting to speculate that these A $\beta$  effects could ultimately threaten the stability of the neuronal genome and interfere with the fine regulation of gene expression required for cognitive functions. Consistent with this notion, genetic ablation of a DNA repair enzyme was recently shown to cause memory deficits in mice<sup>40</sup>.

Some comments are in order on the relative sensitivity of different approaches used to detect DNA damage and related alterations. Extensive DNA damage in proapoptotic or apoptotic cells, such as that caused by severe oxidative stress, can be detected by TUNEL staining<sup>41</sup>. In contrast, neurons of hAPP mice and wildtype controls were not labeled by TUNEL, even when they contained  $\gamma$ H2A.X/53BP1 foci (data not shown), indicating that the TUNEL method is not sensitive enough to detect the level or type of DNA damage that occurs in these mice. Previous reports also indicate that  $\gamma$ H2A.X immunostaining is more sensitive than TUNEL at detecting DSBs<sup>4, 11</sup>. In our study,  $\gamma$ H2A.X immunostaining and the comet assay yielded quantitatively similar results. Relative to baseline measures in the dentate gyrus of wildtype mice, hAPP mice had three times more cells with  $\gamma$ H2A.X-immunoreactive foci and 2.5 times more cells with DNA damage by comet assay. These assays provide qualitatively distinct and complementary types of information. For example, the double labeling of brain sections with antibodies to  $\gamma$ H2A.X and NeuN allowed us to determine that most cells with DSBs in wildtype and hAPP mice, before and after exploration of a novel environment, were neurons. After exploration, hAPP mice had similar numbers of neurons with DSBs as did wildtype controls, as shown by  $\gamma$ H2A.X immunostaining, but more severe DNA fragmentation per cell, as shown by comet assay.

Several studies suggest that A $\beta$  oligomers and AD can cause neurons to re-enter the cell cycle<sup>42, 43</sup>. However, neuronal cell cycle events in APP transgenic mice have not been reported before 6 months of age and appear to be more prominent in the brain stem and frontal cortex than the dentate gyrus. Furthermore, they appear to be absent in adult wildtype mice. Therefore, it is unlikely that cell cycle re-entry caused the neuronal  $\gamma$ H2A.X/53BP1 foci we observed in wildtype and hAPP mice, which were most abundant in the dentate gyrus and detectable in hAPP mice by 1.5 months of age. However, it is possible that chronic increases in DNA damage ultimately promote cell cycle events.

We found the greatest number of neurons with exploration-induced DSBs in the dentate gyrus, a brain region critically involved in spatial learning and memory. Since exposure to three brief electroconvulsive seizures did not increase the number of DSBs in the dentate gyrus of rats<sup>12</sup>, it is remarkable that a natural animal behavior clearly increased DSBs in this region. In all brain regions examined, the DSBs in wildtype mice were transient (lasting <24 hours), indicating efficient repair. Therefore, our snap-shot measurements likely underestimate the total number of DSBs that occur in neurons over time. We hypothesize that the formation of DSBs in neurons is a natural process that facilitates the extensive chromatin remodeling and changes in gene expression involved in information processing, learning and memory. However, we cannot exclude the possibility that the DSBs are merely a byproduct of energy metabolism in particularly active neurons.

We obtained several lines of evidence in support of the hypothesis that both exploratory behavior and pathologically elevated levels of A $\beta$  increase neuronal DSBs by modulating neuronal activity: (1) increasing neuronal activity by visual stimulation in the absence of active behaviors or by optogenetic stimulation in behaving mice was sufficient to increase neuronal DSBs, (2) interventions that suppress aberrant network activity in hAPP mice<sup>30, 34</sup> normalized their levels of neuronal DSBs, and (3) A $\beta$  oligomers no longer increased neuronal DSBs in primary cultures when neuronal activity was blocked.

Our findings that tau ablation in hAPP mice prevented both baseline and exploration-associated abnormalities in neuronal DSBs suggest that endogenous tau has an essential role in their accumulation. Tau ablation also prevents many other problems in this and other lines of hAPP mice, including aberrant network activity, changes in activity-related proteins, deficits in synaptic functions, impairments in learning and memory, and behavioral alterations<sup>19, 30, 33</sup>. Furthermore, in mice without hAPP, tau ablation had very limited effects on neuronal  $\gamma$ H2A.X foci (this study) and on a wide range of other measures<sup>33, 44</sup>, supporting the notion that tau reduction may be of specific benefit in AD.

The precise mechanisms by which tau enables A $\beta$ -induced neuronal dysfunction remain to be determined; however, several lines of evidence suggest that permission or promotion of aberrant excitatory neuronal activity is critically involved<sup>17-19, 30</sup>. Consistent with this notion, we found that treatment with the anti-epileptic drug levetiracetam also reduced abnormalities in neuronal  $\gamma$ H2A.X foci in hAPP mice.

We used primary cultures to confirm that A $\beta$  oligomers alone can cause neuronal DSBs and to explore the mechanisms underlying this phenomenon. Several mechanisms have been

proposed to explain how A $\beta$  oligomers may cause aberrant neuronal activity and impair synaptic functions<sup>18, 45</sup>. Most pertinent to the current study, A $\beta$  oligomers lead to excessive activation of extrasynaptic NMDARs<sup>36, 46</sup>, which could trigger aberrant excitatory neuronal activity as well as synaptic depression<sup>18, 35</sup>, both of which are observed in hAPP mice<sup>17, 45</sup>. In neuronal cultures, we were able to prevent A $\beta$  oligomer-induced increases in neuronal DSBs by blocking extrasynaptic NR2B-containing NMDARs. These results suggest that activation of NR2B-containing extrasynaptic NMDARs contributes causally to the formation of A $\beta$ - and neuronal activity-dependent DSBs, and that selective blockade of these receptors may help protect and stabilize the neuronal genome in disease-related contexts.

In the absence of A $\beta$  oligomers, the number of DSBs transiently increased following stimulation of cultured neurons with NMDA, but fell back to baseline levels within a few hours (Fig. S5b)<sup>11</sup>. However, in the presence of A $\beta$  oligomers, or when intrasynaptic NMDARs were blocked pharmacologically, stimulation with NMDA prolonged the elevation in DSBs (Fig. 8d). These findings suggest that stimulation of intrasynaptic NMDARs is required for the efficient repair of activity-induced neuronal DSBs and that A $\beta$  oligomers interfere with this process. Consistent with these *in vitro* findings, hAPP mice showed an abnormal persistence of exploration-induced DSB in the dentate gyrus and parietal cortex, brain regions that are severely affected by AD.

What molecular mechanisms might link NMDAR stimulation to the formation of DSBs in physiological and pathophysiological contexts? Increasing the balance between extrasynaptic versus intrasynaptic NMDAR activity might alter downstream signaling cascades and calcium influx in ways that promote aberrant activation of endonucleases, circumscribed increases in free radical production, or inhibition/failure of the DNA repair machinery. These possibilities are not mutually exclusive and deserve to be further explored in future studies. The endonuclease SPO11 generates physiological DSBs during meiosis in the testis<sup>23</sup>. The increase in its levels we observed in the dentate gyrus of wildtype mice that had explored a novel environment suggests that SPO11 may be involved in the generation of activity-induced DSBs in neurons.

Oxidative stress can cause DSBs<sup>5</sup>, but hAPP-J20 mice show no evidence of increased oxidative stress in the brain at the ages analyzed here<sup>47</sup>. In rat cortical cultures, transient glutamate-induced neuronal DNA damage was reduced by pretreatment with a mitochondrial superoxide dismutase mimetic<sup>48</sup>, but this study focused on single strand breaks and base oxidation and did not specifically address neuronal DSBs. Although stimulation of NMDA receptors in the extrasynaptic condition increased both ROS and  $\gamma$ H2A.X levels in our neuronal cultures, pretreatment of these cultures with an ROS scavenger reduced the increase in ROS production but not the increase in  $\gamma$ H2A.X levels, diminishing the likelihood that ROS are a critical mediator of activity-induced DSBs. However, the methods we used are not sensitive enough to rule out more circumscribed and transient increases in ROS production in specific subcellular compartments.

In light of other evidence that histone and chromatin modifications are important in both cognition and memory disorders<sup>49, 50</sup>, it is tempting to speculate that A $\beta$ -induced

abnormalities in the formation and repair of DSBs similar to those we identified in hAPP mice and neuronal cultures may contribute to AD-related neurological deficits (Fig. S8). Additional research is needed to test the hypothetical framework depicted in this figure and to assess the roles of neuronal DSBs in health and disease.

## METHODS

### Mice and tissues

We studied 4–7-month-old heterozygous hAPP transgenic and wildtype mice from line J20 on a *Tau*<sup>+/+</sup>, *Tau*<sup>+/-</sup>, or *Tau*<sup>-/-</sup> C57Bl/6J background. Transgenic C57Bl/6J mice expressing Cre-recombinase in medium spiny neurons of the indirect pathway in the dorsomedial striatum directed by A2<sub>A</sub> receptor regulatory elements (A2A-Cre mice) were from GENSAT. Eight-week-old adrenalectomized versus sham-operated wildtype mice were obtained from the Jackson Laboratory. All *in vivo* analyses were carried out on sex-matched or sex-balanced groups. Mice were anesthetized with Avertin (tribromoethanol, 250 mg/kg) and perfused transcardially with 0.9% NaCl. One hemibrain was snap frozen and stored at -80°C. The other was drop-fixed in 4% paraformaldehyde in phosphate-buffered saline (PBS) and sectioned into 30 µm-thick slices using a sliding microtome (Leica SM2000R). After visual and optogenetic stimulation, both hemibrains were fixed with paraformaldehyde. All animal experiments were approved by the Institutional Animal Care and Use Committee of the University of California, San Francisco.

### Antibodies and other reagents

Primary antibodies used included monoclonal mouse anti-γH2A.X (JBW301), anti-NeuN biotinylated (MAB377B) (Millipore) and anti-α-tubulin (B5-1-2, Sigma-Aldrich), and polyclonal rabbit anti-MAP2 (AB5622) (Millipore), anti-phospho-ERK1/2 (9101) and anti-total ERK1/2 (4696) (Cell Signaling Technology), anti-53BP1 (NB100304) and anti-SPO-11 (NBP1-58172) (Novus Biologicals). Synthetic Aβ1-42 oligomers were prepared from lyophilized monomers (rPeptide or Biopeptide) and naturally secreted Aβ oligomers were isolated from stably hAPP-transfected CHO-7PA2 cells<sup>45</sup>. Tetrodotoxin (TTX), bicuculline, NMDA and the following inhibitors of glutamate receptors were from Tocris: 2,3-dihydroxy-6-nitro-7-sulfamoylbenzo[f]quinoxaline-2,3-dione (NBQX), (2R)-amino-5-phosphonovaleric acid (APV), dizocilpine (MK801), and ifenprodil. Levetiracetam (UCB Pharmaceuticals) was infused continuously with subcutaneous Alzet minipumps<sup>34</sup>.

### Cell cultures and treatments

Primary cultures of hippocampal and cortical neurons established from postnatal day-0 pups<sup>45, 51</sup> were plated on dishes (BD Falcon) (10<sup>6</sup> cells/35-mm dish) or glass coverslips (Bellco Glass) (150,000 cells/12-mm coverslip) coated with poly-L lysine (Sigma-Aldrich) and laminin (Roche). Cultures were used for experiments after 14 days *in vitro* (DIV) and incubated at 37°C during all treatments. They were incubated overnight with NBQX (50 µM) and D-AP5 (100 µM). Cells were then rinsed with warm PBS and incubated for 60 min at 37°C in neuron-conditioned medium that did or did not contain TTX (1 µM), or NBQX (50 µM) and/or D-AP5 (100 µM), followed by addition of Aβ oligomers (1 µM) or vehicle. After 5 h, cells were processed for western blot analysis or immunofluorescence staining.

To examine the roles of intrasynaptic versus extrasynaptic NMDA receptors, cells were incubated with TTX (1  $\mu$ M), NBQX (50  $\mu$ M) and D-AP5 (100  $\mu$ M) for 24 h. They were then washed in warm PBS and incubated in neuron-conditioned medium for 30–60 min to remove the inhibitors and prevent them from interfering with stimulation of glutamate receptors. A $\beta$  oligomers (1  $\mu$ M) or vehicle was added to the cultures 10 min before stimulation. At this time, half of the medium was collected from each well and kept at 37°C (conditioned medium).

To activate synaptic NMDARs (“intrasynaptic” or IntraS protocol), neurons were disinhibited with 10  $\mu$ M bicuculline for 10 min, rinsed with warm PBS, and incubated in their conditioned medium. To activate extrasynaptic NMDARs (“extrasynaptic” or ExtraS protocol), neurons were incubated in medium containing MK801 (40  $\mu$ M) and bicuculline (10  $\mu$ M) for 10 min, rinsed with warm PBS, incubated in medium containing NMDA (10  $\mu$ M) for 5 min, washed and then incubated in their conditioned medium. Five hours later, cells were processed for western blot analysis or immunofluorescence staining. For specific inhibition of NR2B-containing NMDARs, the extrasynaptic protocol was modified by adding ifenprodil (3  $\mu$ M) to all steps, starting with the overnight inhibitor pretreatment.

### Western blot analysis

Frozen hemibrains from perfused mice were microdissected in ice-cold PBS containing complete protease inhibitors (Roche) and homogenized in RIPA buffer (10 mM Tris/HCl, pH 7.5, 50 mM NaCl, 30 mM Na<sub>4</sub>P<sub>2</sub>O<sub>7</sub>, 5  $\mu$ M ZnSO<sub>4</sub>, 10% glycerol, 0.1% SDS, 1% Triton X-100, 1 mM dithiothreitol) containing complete protease inhibitors and a cocktail of phosphatase inhibitors (Sigma-Aldrich). Cultured cells were washed in PBS and scraped into RIPA buffer. Lysates were sonicated for 5 min at 4°C and spun in a refrigerated microcentrifuge at maximal speed for 10 min. Protein concentrations were determined by Bradford assay. Proteins (20  $\mu$ g per sample) were loaded on 4–12% Bis-Tris gels (Invitrogen), separated by SDS-PAGE, and transferred to nitrocellulose membranes. After 1 h in blocking solution (5% nonfat milk in TBS), membranes were incubated with primary antibodies. Blots were washed 3 times in TBS/0.1% Tween and incubated with secondary IRD-tagged antibodies (800 IRDye and 680 IRDye) (Li-COR, Lincoln, NE) in Odyssey blocking buffer for 1 h at room temperature (RT). Western blot signals were analyzed with an Odyssey Li-COR laser scanning and imaging system (Li-COR, v3.0).

### Behavioral conditions and neuronal stimulation

**Exploration of a novel environment**—Mice were housed in groups of four per cage. Mice in the control group were kept in their original home cages. Mice in the “novel environment” (Novel E) and the “Novel E + recovery” groups were transferred into the testing room and allowed to acclimate to the room for at least 1 h. Each set of 4 group-housed mice was then transferred together into a new cage, which was larger and contained different litter, odors, stations, and toys, and allowed to explore the cage for 2 h. Introducing mice into the novel environment alongside other mice they know well decreases their anxiety and increases their exploratory activity. After the novel environment exploration, mice in the “Novel E” group were killed, whereas mice in the “Novel E + recovery” group were transferred back into their home cages and kept there for 24 h before sacrifice. Half of

the control mice were sacrificed together with the Novel E group and the other half with the Novel E + recovery group.

**Restraint stress**—Each mouse was placed into a 3.0 × 11.5 cm cylinder with porous walls. Pads were added to further restrict space. After 15 min of restraint, the cylinder was placed into an isoflurane chamber. Anesthetized mice were then removed, injected with Avertin, and perfused transcardially within 10 min after the restraint stress ended.

**Visual stimulation**—Mice were anesthetized with 5% isoflurane in a sealed box and placed into a stereotaxic frame in which anesthesia was maintained with isoflurane (0.8%) using a mask. Transparent gel was put on both eyes and one eye was shielded from light with a cap. The other eye was kept open with mini tweezers. Care was taken not to touch the whiskers to avoid stimulation of the barrel field cortex. Visual stimulation consisted of different patterns of horizontal or vertical black-and-white gratings generated by a Powerpoint animation on a computer screen. The screen was positioned 25 cm from the open eye perpendicular to its visual axis. Each pattern was presented 3 times for 0.5 sec with 0.2 sec of darkness between presentations to avoid persistent light exposure. After 15 min of visual stimulation, the screen was shut off and mice were kept in the stereotaxic frame for another 15 min. They were then injected with avertin, removed from isoflurane, and perfused transcardially 30 min later. All procedures were performed under minimal ambient lighting.

**Optogenetic stimulation of the striatum**—Optogenetic stimulation was carried out as described<sup>52</sup>. Briefly, A2A-Cre mice received unilateral stereotaxic striatal injections with adeno-associated virus expressing double-floxed inverted constructs encoding a ChR2-YFP fusion protein or YFP alone. A glass fiber was then implanted close to the viral injection site. Two weeks later, awake mice were placed in a 16" × 16" square box, connected to a 473-nm laser via a 1-meter fiber optic, and stimulated for 1 h with a pattern of 30 sec constant on and 30 sec off (1 mW). All mice were habituated to the box and fiber tethering for 3 days (30–60 min per day) before the laser stimulation. Video tracking of mice during the stimulation sessions and analysis were performed with Ethovision 7.0 software<sup>53</sup> to monitor rotational behaviors. One hour after the end of the stimulation protocol, mice were anesthetized with ketamine and xylazine and transcardially perfused with phosphate buffered saline (PBS), followed by 4% paraformaldehyde. The brains were then processed for immunohistochemistry.

### Immunofluorescence staining

Primary neurons were rinsed with PBS, fixed in 100% methanol for 10 min, and rinsed in Tris-buffered saline (TBS). Coverslips were incubated in blocking solution (5% normal donkey serum in 0.1% TBS-Tween) for 60 min at RT and then overnight at 4°C with anti- $\gamma$ H2A.X and anti-MAP2 antibodies diluted in blocking solution. After rinses with 0.1% TBS-Tween, cells were incubated with corresponding Alexa-conjugated secondary antibodies (1:300, Invitrogen) diluted in 4% normal donkey serum in TBS for 1 h at RT.

Preparation and immunohistochemistry of brain sections were performed essentially as described<sup>29</sup>. However, PBS was replaced with TBS and steps were added for antigen retrieval and peroxidase inhibition to enhance nuclear staining. Sections were incubated overnight at 4°C with primary antibodies (anti- $\gamma$ H2A.X alone or combined with anti-53BP1 or anti-NeuN-biotin). Secondary antibodies were donkey anti-mouse Alexa 488 and anti-rabbit Alexa 593 (Invitrogen), and were used with streptavidin Cy3 (Invitrogen). After extensive rinses, coverslips and sections were mounted with Vectashield mounting medium with DAPI (Vector Laboratories).

Co-localization of  $\gamma$ H2A.X staining and DAPI allowed us to selectively analyze nuclei. Cells containing at least one  $\gamma$ H2A.X-positive focus in the nucleus were counted in four brain regions. For each mouse and brain region, the average number of cells with foci was calculated from counts obtained in three coronal sections. For the optogenetic stimulation experiment, the average number of cells with  $\gamma$ H2A.X-positive foci was calculated from counts obtained in three striatal fields per mouse. Each field was located in a different coronal section and covered an area of viral transduction as judged by the presence of YFP fluorescence.

Digitized images were obtained with an AxioCam HRc camera (Zeiss) mounted on a BX-60 microscope (Olympus) using Axiovision LE software. Confocal images were acquired with an MC04 Zeiss LSM510 multiphoton microscope with Meta software. Stacks of confocal images were deconvoluted with Huygens software. The z-maximum-intensity projection function of ImageJ was used to optimize the appearance of DAPI labels. To visualize  $\gamma$ H2A.X or 53BP1 foci, we selected micrographs within the center of the z-stacks.

### Single cell gel electrophoresis (comet assay)

After perfusion of mice with cold saline, brains were removed rapidly and briefly stored in ice-cold Brains Hibernate A (HA) medium (Brainbits) until micro-dissection. Dentate gyri were isolated in ice-cold HA and homogenized in 1 ml of ice-cold PBS (lacking  $\text{Ca}^{2+}$  and  $\text{Mg}^{2+}$  to inhibit nucleases) by 30 strokes of pipetting. For each sample, 25  $\mu\text{l}$  of homogenate were combined with 250  $\mu\text{l}$  of low-melting point molten agarose (Trevigen), and 50  $\mu\text{l}$  were applied per well on comet slides (Trevigen). All steps were performed within an hour from perfusion. Cell lysis and electrophoretic separation of DNA fragments released from cells were performed according to the instructions included in the CometAssay kit (Trevigen). Comet assays were performed at pH 7.4 because this condition makes the assay more specific for the detection of DSBs<sup>27</sup>. The pH was measured in the TBE buffer used for equilibration and in the TBE buffer of the electrophoresis tank at the beginning and end of the electrophoresis, and was found to be stable in the 7.4–8.0 range. Single-cell gel electrophoresis was performed at 1 volts/cm for 40 minutes. SYBR green was used to fluorescently stain the comet-like smears of DNA fragments that emerged from cells containing DSBs. Digitized images were obtained with an AxioCam HRc camera (Zeiss) mounted on a BX-60 microscope (Olympus) using Axiovision LE software and analyzed with CometScore software (Tritek). For each sample, the number of cells with comets was counted manually in 2–3 fields and normalized to the total number of cells in the fields. For each field, at least 150 cells were inspected. For each comet detected, the comet was framed

and a cursor adjusted on the head of the comet via the selection tool of the software. The software automatically determined the tail length and percent DNA in the tail using a built-in algorithm for comet scoring. For each field, the experimenter calculated the average value of the tail length, sorted the proportion of DNA in the tail in three categories (<20%, 20% to <40%, 40%), and calculated the proportion of comet-bearing cells in each of these categories.

### **Whole body $\gamma$ -irradiation**

Two to four mice were positioned evenly in a container with individual casings and placed on the rotating support of a Mark I, series-30  $\gamma$ -irradiator with a 5,500 curie cesium-137 source (J.S. Shepherd and Associates). They received 0, 1, 2, 5 or 10 Gy of whole body  $\gamma$ -irradiation. All mice spent the same amount of time in the irradiator as doses were determined by the progressive removal of attenuators (x2, x5, x10). After irradiation, mice were put back into their home cages for 1 h before anesthesia and transcardial perfusion. One hemibrain was processed for neutral pH comet assay and the other for immunohistochemistry.

### **Measurement of plasma corticosterone levels by ELISA**

Mice were anesthetized with isoflurane (5% in sealed cage) and injected with Avertin to maintain anesthesia during terminal transcardial perfusions. Blood was collected centrally by puncture of the heart into heparin-coated tubes and centrifuged at 2000 rpm for 8 min at 4°C. Plasma was collected and frozen at -80°C until measurement of corticosterone levels with an ELISA kit (ENZO Life Sciences) according to the manufacturer's instructions. Mice were perfused with 0.9% saline and their brains processed for immunohistochemistry.

### **Assessment of ROS production by live fluorescence microscopy**

Neurons grown on coverslips (14 DIV) were pre-treated for 1 h with 20  $\mu$ M of the ROS scavenger Euk-134<sup>54,55</sup>; (Cayman Chemicals) or vehicle (DMSO), followed by the treatments indicated in Fig. 8a. 100  $\mu$ M of H<sub>2</sub>O<sub>2</sub> was used as a positive control for ROS induction. One and a half hour after the end of these treatments, cultures were incubated with 2  $\mu$ M of the ROS indicator CM-H2CFDA (Invitrogen) for 40 min, with addition of 4  $\mu$ M of Hoechst 33342 (Thermo Scientific) during the last 5 min, and then rinsed twice with warm tyrode buffer (126.5 mM NaCl, 2.5 mM KCl, 2 mM CaCl<sub>2</sub>, 2 mM MgCl<sub>2</sub>, 10 mM HEPES, 30 mM glucose, pH 7.4). A fluorescence microscope (Nikon eclipse Ti) equipped with a chamber maintained at 37°C was used to image the live neurons. Images were acquired with Metamorph software (version 7.7.3.0). The plug-in module for particle counting from Image J was used to automatically count the number of Hoechst 33342-labeled nuclei. Nuclei colabeled with CM-H2CFDA were counted manually.

### **Blind-coding and statistical analysis**

Investigators who obtained data were blinded with respect to the genotype and treatment of mice and cell cultures. Sample sizes were chosen based on pilot experiments and previous experience with similar types of experiments. Statistical analyses were performed with GraphPad Prism, SPSS, or R (R Development Core Team, 2011). Normal distribution of the

data was verified by D'Agostino and Pearson omnibus normality test. Differences between two means were assessed by unpaired or paired Student's *t*-test. Differences among multiple means were assessed, as indicated, by one-way or two-way ANOVA, followed by Tukey's, Dunnett's, Bonferroni's, or Dunn's *post-hoc* tests. For the statistical analysis in Fig. S2, factors were assessed by a four-way repeated measures ANOVA and a corresponding linear mixed model (package nlme)<sup>56</sup> that accounted for the effect of repeated measures obtained in the brains of the same mice. Null hypotheses were rejected at the 0.05 level.

## Supplementary Material

Refer to Web version on PubMed Central for supplementary material.

## Acknowledgements

We thank D. J. Selkoe and D. Walsh for CHO-7PA2 cells; N. Sakane, E. Verdin and L. Verret for helpful comments on the manuscript; H. Kassler for advice on  $\gamma$ -irradiation; D. Davalos for advice on confocal imaging; Divya Pathak for advice on live cell imaging; H. Solanoy, M. Thwin, C. Wang and G.-Q. Yu for technical support; A.L. Lucido for editorial review; J. Carroll, T. Roberts, G. Maki and C. Goodfellow for preparation of graphics; and M. Dela Cruz for administrative assistance. The study was supported by NIH grants AG011385, AG022074 and NS065780 to L.M. and a gift from the S.D. Bechtel, Jr. Foundation.

## REFERENCES

1. Brasnjevic I, Hof PR, Steinbusch HW, Schmitz C. Accumulation of nuclear DNA damage or neuron loss: Molecular basis for a new approach to understanding selective neuronal vulnerability in neurodegenerative diseases. *DNA Repair (Amst)*. 2008; 7:1087–1097. [PubMed: 18458001]
2. Moreira PI, et al. Nucleic acid oxidation in Alzheimer disease. *Free Radic. Biol. Med*. 2008; 44:1493–1505. [PubMed: 18258207]
3. Lu T, et al. Gene regulation and DNA damage in the ageing human brain. *Nature*. 2004; 429:883–891. [PubMed: 15190254]
4. Bonner WM, et al. GammaH2AX and cancer. *Nat. Rev. Cancer*. 2008; 8:957–967. [PubMed: 19005492]
5. Ismail IH, Hendzel MJ. The gamma-H2A.X: Is it just a surrogate marker of double-strand breaks or much more? *Environ. Mol. Mutagen*. 2008; 49:73–82. [PubMed: 18095327]
6. Kim D, et al. Deregulation of HDAC1 by p25/Cdk5 in neurotoxicity. *Neuron*. 2008; 60:803–817. [PubMed: 19081376]
7. Fernandez-Capetillo O, et al. H2AX is required for chromatin remodeling and inactivation of sex chromosomes in male mouse meiosis. *Dev. Cell*. 2003; 4:497–508. [PubMed: 12689589]
8. Lee SY, et al. Histone XH2AX is required for *Xenopus* anterior neural development: Critical role of threonine 16 phosphorylation. *J. Biol. Chem*. 2010; 285:29525–29534. [PubMed: 20639511]
9. Yin B, et al. Histone H2AX stabilizes broken DNA strands to suppress chromosome breaks and translocations during V(D)J recombination. *J. Exp. Med*. 2009; 206:2625–2639. [PubMed: 19887394]
10. Fernando RN, et al. Cell cycle restriction by histone H2AX limits proliferation of adult neural stem cells. *Proc. Natl. Acad. Sci. USA*. 2011; 108:5837–5842. [PubMed: 21436033]
11. Crowe SL, Movsesyan VA, Jorgensen TJ, Kondratyev A. Rapid phosphorylation of histone H2A.X following ionotropic glutamate receptor activation. *Eur. J. Neurosci*. 2006; 23:2351–2361. [PubMed: 16706843]
12. Crowe SL, Tsukerman S, Gale K, Jorgensen TJ, Kondratyev AD. Phosphorylation of histone H2A.X as an early marker of neuronal endangerment following seizures in the adult rat brain. *J. Neurosci*. 2011; 31:7648–7656. [PubMed: 21613478]

13. Palop JJ, et al. Vulnerability of dentate granule cells to disruption of Arc expression in human amyloid precursor protein transgenic mice. *J. Neurosci.* 2005; 25:9686–9693. [PubMed: 16237173]
14. Vazdarjanova A, et al. Spatial exploration induces ARC, a plasticity-related immediate-early gene, only in calcium/calmodulin-dependent protein kinase II-positive principal excitatory and inhibitory neurons of the rat forebrain. *J. Comp. Neurol.* 2006; 498:317–329. [PubMed: 16871537]
15. Cheng I, et al. Accelerating amyloid- $\beta$  fibrillization reduces oligomer levels and functional deficits in Alzheimer disease mouse models. *J. Biol. Chem.* 2007; 282:23818–23828. [PubMed: 17548355]
16. Palop JJ, et al. Neuronal depletion of calcium-dependent proteins in the dentate gyrus is tightly linked to Alzheimer's disease-related cognitive deficits. *Proc. Natl. Acad. Sci. USA.* 2003; 100:9572–9577. [PubMed: 12881482]
17. Palop JJ, et al. Aberrant excitatory neuronal activity and compensatory remodeling of inhibitory hippocampal circuits in mouse models of Alzheimer's disease. *Neuron.* 2007; 55:697–711. [PubMed: 17785178]
18. Palop JJ, Mucke L. Amyloid-beta-induced neuronal dysfunction in Alzheimer's disease: From synapses toward neural networks. *Nat. Neurosci.* 2010; 13:812–818. [PubMed: 20581818]
19. Roberson ED, et al. Reducing endogenous tau ameliorates amyloid  $\beta$ -induced deficits in an Alzheimer's disease mouse model. *Science.* 2007; 316:750–754. [PubMed: 17478722]
20. Gotz J, Ittner LM. Animal models of Alzheimer's disease and frontotemporal dementia. *Nat. Rev. Neurosci.* 2008; 9:532–544. [PubMed: 18568014]
21. Kobayashi DT, Chen KS. Behavioral phenotypes of amyloid-based genetically modified mouse models of Alzheimer's Disease. *Genes Brain Behav.* 2005; 4:173–196. [PubMed: 15810905]
22. Marchetti C, Marie H. Hippocampal synaptic plasticity in Alzheimer's disease: What have we learned so far from transgenic models? *Rev. Neurosci.* 2011; 22:373–402. [PubMed: 21732714]
23. Lange J, et al. ATM controls meiotic double-strand-break formation. *Nature.* 2011; 479:237–240. [PubMed: 22002603]
24. Fillingham J, Keogh MC, Krogan NJ.  $\gamma$ H2AX and its role in DNA double-strand break repair. *Biochem. Cell Biol.* 2006; 84:568–577. [PubMed: 16936829]
25. Anderson L, Henderson C, Adachi Y. Phosphorylation and rapid relocalization of 53BP1 to nuclear foci upon DNA damage. *Mol. Cell Biol.* 2001; 21:1719–1729. [PubMed: 11238909]
26. Ward IM, Minn K, Jorda KG, Chen J. Accumulation of checkpoint protein 53BP1 at DNA breaks involves its binding to phosphorylated histone H2AX. *J. Biol. Chem.* 2003; 278:19579–19582. [PubMed: 12697768]
27. Olive PL, Banath JP. The comet assay: A method to measure DNA damage in individual cells. *Nat. Protoc.* 2006; 1:23–29. [PubMed: 17406208]
28. Flint MS, Baum A, Chambers WH, Jenkins FJ. Induction of DNA damage, alteration of DNA repair and transcriptional activation by stress hormones. *Psychoneuroendocrinology.* 2007; 32:470–479. [PubMed: 17459596]
29. Harris JA, et al. Transsynaptic progression of amyloid- $\beta$ -induced neuronal dysfunction within the entorhinal-hippocampal network. *Neuron.* 2010; 68:428–441. [PubMed: 21040845]
30. Roberson ED, et al. Amyloid- $\beta$ /Fyn-induced synaptic, network, and cognitive impairments depend on Tau levels in multiple mouse models of Alzheimer's disease. *J. Neurosci.* 2011; 31:700–711. [PubMed: 21228179]
31. Verret L, et al. Inhibitory interneuron deficit links altered network activity and cognitive dysfunction in Alzheimer model. *Cell.* 2012; 149:708–721. [PubMed: 22541439]
32. Palop JJ, Mucke L. Epilepsy and cognitive impairments in Alzheimer disease. *Arch. Neurol.* 2009; 66:435–440. [PubMed: 19204149]
33. Morris M, Maeda S, Vossel K, Mucke L. The many faces of tau. *Neuron.* 2011; 70:410–426. [PubMed: 21555069]
34. Sanchez PE, et al. Levetiracetam suppresses neuronal network dysfunction and reverses synaptic and cognitive deficits in an Alzheimer's disease model. *Proc. Natl. Acad. Sci. USA.* 2012; 109:E2895–E2903. [PubMed: 22869752]

35. Hardingham GE, Bading H. Synaptic versus extrasynaptic NMDA receptor signalling: Implications for neurodegenerative disorders. *Nat. Rev. Neurosci.* 2010; 11:682–696. [PubMed: 20842175]
36. Li S, et al. Soluble A $\beta$  oligomers inhibit long-term potentiation through a mechanism involving excessive activation of extrasynaptic NR2B-containing NMDA receptors. *J. Neurosci.* 2011; 31:6627–6638. [PubMed: 21543591]
37. Shull ER, et al. Differential DNA damage signaling accounts for distinct neural apoptotic responses in ATLD and NBS. *Genes Dev.* 2009; 23:171–180. [PubMed: 19171781]
38. Bhogal N, Jalali F, Bristow RG. Microscopic imaging of DNA repair foci in irradiated normal tissues. *Int. J. Radiat. Biol.* 2009; 85:732–746. [PubMed: 19296345]
39. Grudzenski S, Raths A, Conrad S, Rube CE, Loblrich M. Inducible response required for repair of low-dose radiation damage in human fibroblasts. *Proc. Natl. Acad. Sci. USA.* 2010; 107:14205–14210. [PubMed: 20660770]
40. Canugovi C, et al. Endonuclease VIII-like 1 (NEIL1) promotes short-term spatial memory retention and protects from ischemic stroke-induced brain dysfunction and death in mice. *Proc. Natl. Acad. Sci. USA.* 2012; 109:14948–14953. [PubMed: 22927410]
41. Zhang Y, Goodyer C, LeBlanc A. Selective and protracted apoptosis in human primary neurons microinjected with active caspase-3, -6, -7, and -8. *J. Neurosci.* 2000; 20:8384–8389. [PubMed: 11069945]
42. Lee HG, et al. Cell cycle re-entry mediated neurodegeneration and its treatment role in the pathogenesis of Alzheimer's disease. *Neurochem. Int.* 2009; 54:84–88. [PubMed: 19114068]
43. Li L, Cheung T, Chen J, Herrup K. A comparative study of five mouse models of Alzheimer's disease: Cell cycle events reveal new insights into neurons at risk for death. *Int. J. Alzheimers Dis.* 2011; 2011:171464. [PubMed: 21912750]
44. Morris M, Koyama A, Masliah E, Mucke L. Tau reduction does not prevent motor deficits in two mouse models of Parkinson's disease. *PLoS One.* 2011; 6:e29257. [PubMed: 22206005]
45. Cisse M, et al. Reversing EphB2 depletion rescues cognitive functions in Alzheimer model. *Nature.* 2011; 469:47–52. [PubMed: 21113149]
46. Li S, et al. Soluble oligomers of amyloid  $\beta$ -protein facilitate hippocampal long-term depression by disrupting neuronal glutamate uptake. *Neuron.* 2009; 62:788–801. [PubMed: 19555648]
47. Esposito L, et al. Reduction in mitochondrial superoxide dismutase modulates Alzheimer's disease-like pathology and accelerates the onset of behavioral changes in human amyloid precursor protein transgenic mice. *J. Neurosci.* 2006; 26:5167–5179. [PubMed: 16687508]
48. Yang JL, Tadokoro T, Keijzers G, Mattson MP, Bohr VA. Neurons efficiently repair glutamate-induced oxidative DNA damage by a process involving CREB-mediated up-regulation of apurinic endonuclease 1. *J. Biol. Chem.* 2010; 285:28191–28199. [PubMed: 20573957]
49. Day JJ, Sweatt JD. Epigenetic mechanisms in cognition. *Neuron.* 2011; 70:813–829. [PubMed: 21658577]
50. Graff J, Kim D, Dobbin MM, Tsai LH. Epigenetic regulation of gene expression in physiological and pathological brain processes. *Physiol. Rev.* 2011; 91:603–649. [PubMed: 21527733]
51. Cheng JS, et al. Collagen VI protects neurons against A $\beta$  toxicity. *Nat. Neurosci.* 2009; 12:119–121. [PubMed: 19122666]
52. Kravitz AV, et al. Regulation of parkinsonian motor behaviours by optogenetic control of basal ganglia circuitry. *Nature.* 2010; 466:622–626. [PubMed: 20613723]
53. Spink AJ, Tegelenbosch RAJ, Buma MOS, Noldus LPJJ. The EthoVision video tracking system - A tool for behavioral phenotyping of transgenic mice. *Physiol. Behav.* 2001; 73:731–744. [PubMed: 11566207]
54. Pong K, Doctrow SR, Huffman K, Adinolfi CA, Baudry M. Attenuation of staurosporine-induced apoptosis, oxidative stress, and mitochondrial dysfunction by synthetic superoxide dismutase and catalase mimetics, in cultured cortical neurons. *Exp. Neurol.* 2001; 171:84–97. [PubMed: 11520123]
55. Rong Y, Doctrow SR, Tocco G, Baudry M. EUK-134, a synthetic superoxide dismutase and catalase mimetic, prevents oxidative stress and attenuates kainate-induced neuropathology. *Proc. Natl. Acad. Sci. USA.* 1999; 96:9897–9902. [PubMed: 10449791]

56. Pinheiro J, Bates D, DebRoy S, Sarkar D, R Development Core Team. nlme: Linear and Nonlinear Mixed Effects Models. R package version 3.1-102. 2011

Author Manuscript

Author Manuscript

Author Manuscript

Author Manuscript

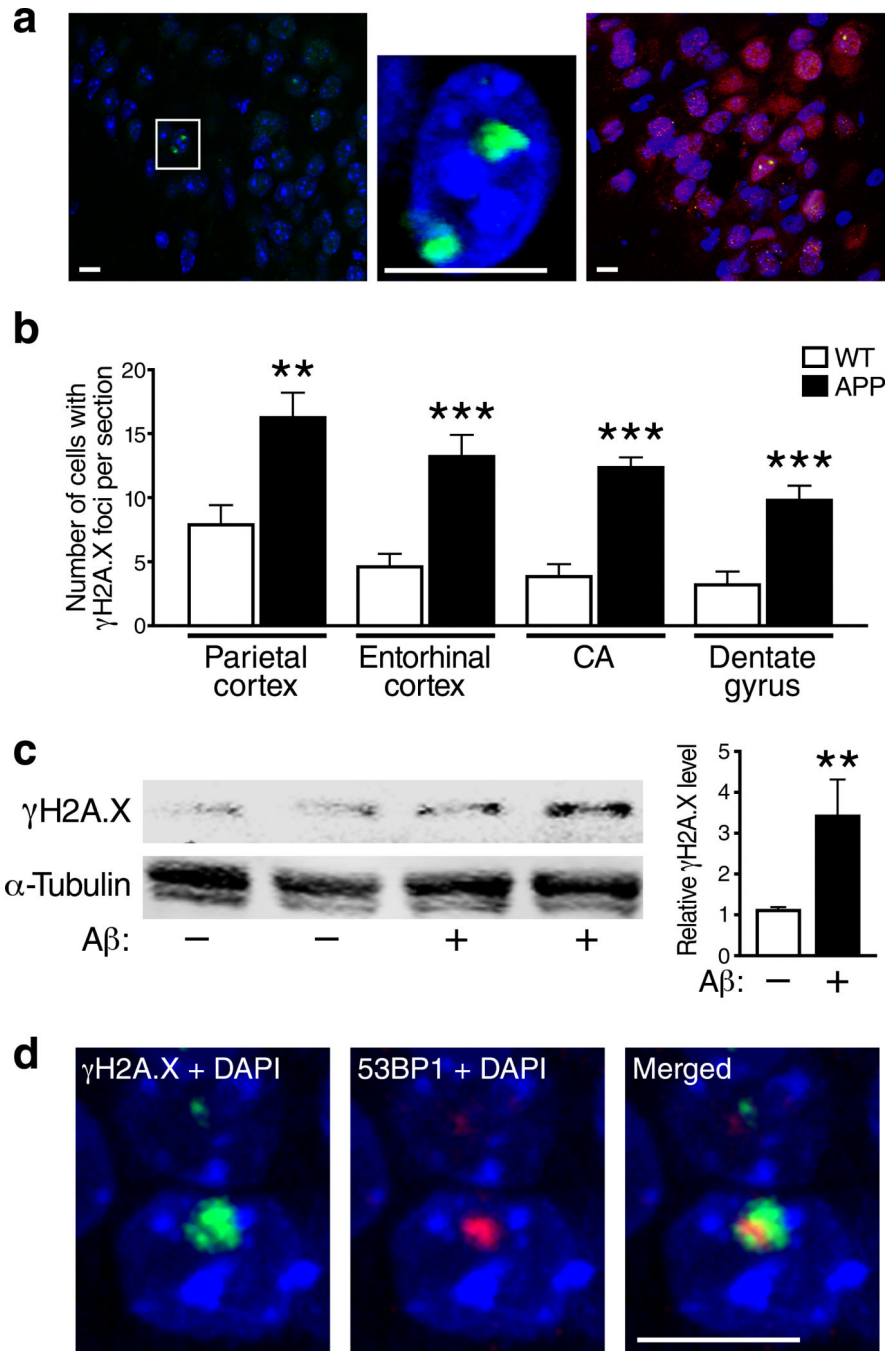


**Figure 1. A $\beta$  increases neuronal  $\gamma$ H2A.X formation *in vivo* and *in vitro***

(a, b)  $\gamma$ H2A.X-positive foci in immunostained brain sections from 6-month-old wildtype and hAPP mice were visualized by confocal microscopy. (a)  $\gamma$ H2A.X-positive foci (green) were localized in nuclei labeled with DAPI (blue) and were found primarily in cells co-labeled with an antibody to the neuronal marker NeuN (red, right panel). The middle panel shows a higher magnification image of the area within the white box in the left panel. Images were taken from the entorhinal cortex of an hAPP mouse. Scale bars: 10  $\mu$ m. (b) Numbers of cells with  $\gamma$ H2A.X-positive foci per section in different brain regions of

wildtype (WT) and hAPP (APP) mice (n=8 mice/genotype). **(c)** Cultures of primary forebrain neurons from wildtype mice were exposed to A $\beta$  oligomers (1  $\mu$ M)(+) or vehicle (-) for 4 h.  $\gamma$ H2A.X levels were then determined by western blot analysis.  $\alpha$ -Tubulin served as a loading control. A representative western blot is shown on the left and quantifications of western blot signals on the right (n=8–12 wells per condition from 4 independent experiments). **(d)** Representative example of an  $\gamma$ H2A.X-positive focus (green) double-labeled with anti-53BP1 (red) in a DAPI-labeled (blue) neuronal nucleus in the dentate gyrus of a 6-month-old hAPP mouse. \*\*p<0.01, \*\*\*p<0.001 (two-tailed, unpaired Student's *t*-test). Bars represent means  $\pm$  SEM.

Author Manuscript

Author Manuscript

Author Manuscript

Author Manuscript



mice exposed to the home cage condition (Bonferroni *post-hoc* test). Bars represent means  $\pm$  SEM.

Author Manuscript

Author Manuscript

Author Manuscript

Author Manuscript

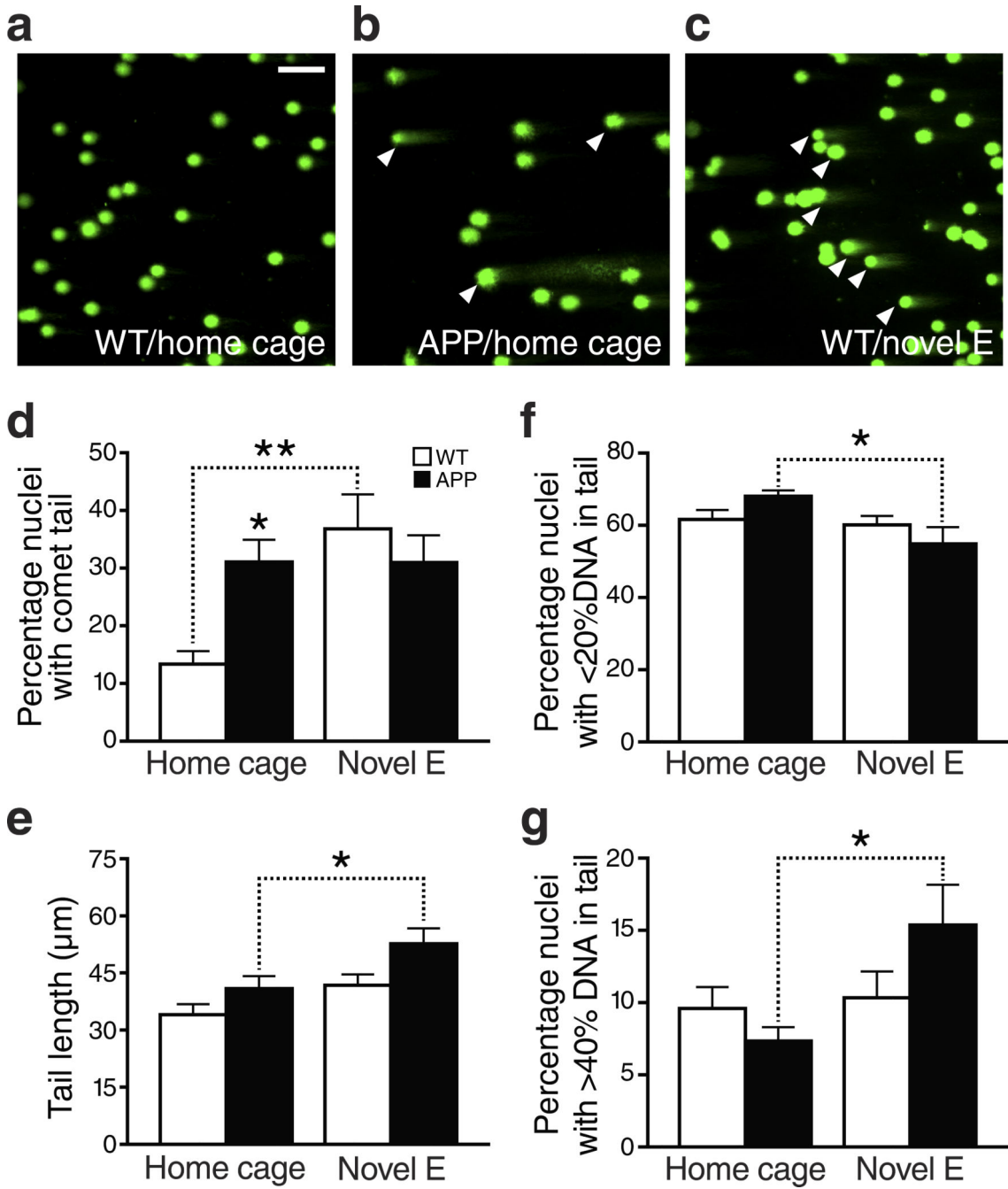


**Figure 3. Exploration- and hAPP/A $\beta$ -induced increases in DNA damage detected by the comet assay**  
 Cells isolated from dentate gyrus homogenates were assessed for DSB levels by the comet assay at neutral pH. (a–c) Representative images of cell nuclei from wildtype (a) and hAPP (b) mice taken from their home cage (control condition), and from a wildtype mouse that had just explored a novel environment (Novel E) for 2 hours (c). DNA of the agarose-embedded nuclei was stained with SYBR-green after separation of DNA fragments by electrophoresis. Images were captured by fluorescence microscopy. Scale bar: 50  $\mu$ m. (d) Quantification of the percentage of nuclei with comet tails, which are indicative of DSBs.

For each mouse, a total of 600-800 nuclei within 2 fields were inspected and scored. **(e)** Tail length (in  $\mu\text{m}$ ), indicating the extent of DNA fragmentation, was measured for each cell showing a comet. **(f, g)** Proportion of comet-bearing nuclei with  $<20\%$  **(f)** or  $>40\%$  **(g)** fragmented DNA.  $n=6-9$  mice per genotype and condition.  $*p<0.05$  ,  $**p<0.01$  vs. leftmost bar or as indicated by bracket (Bonferroni *post-hoc* test). Bars represent means  $\pm$  SEM.

Author Manuscript

Author Manuscript

Author Manuscript

Author Manuscript

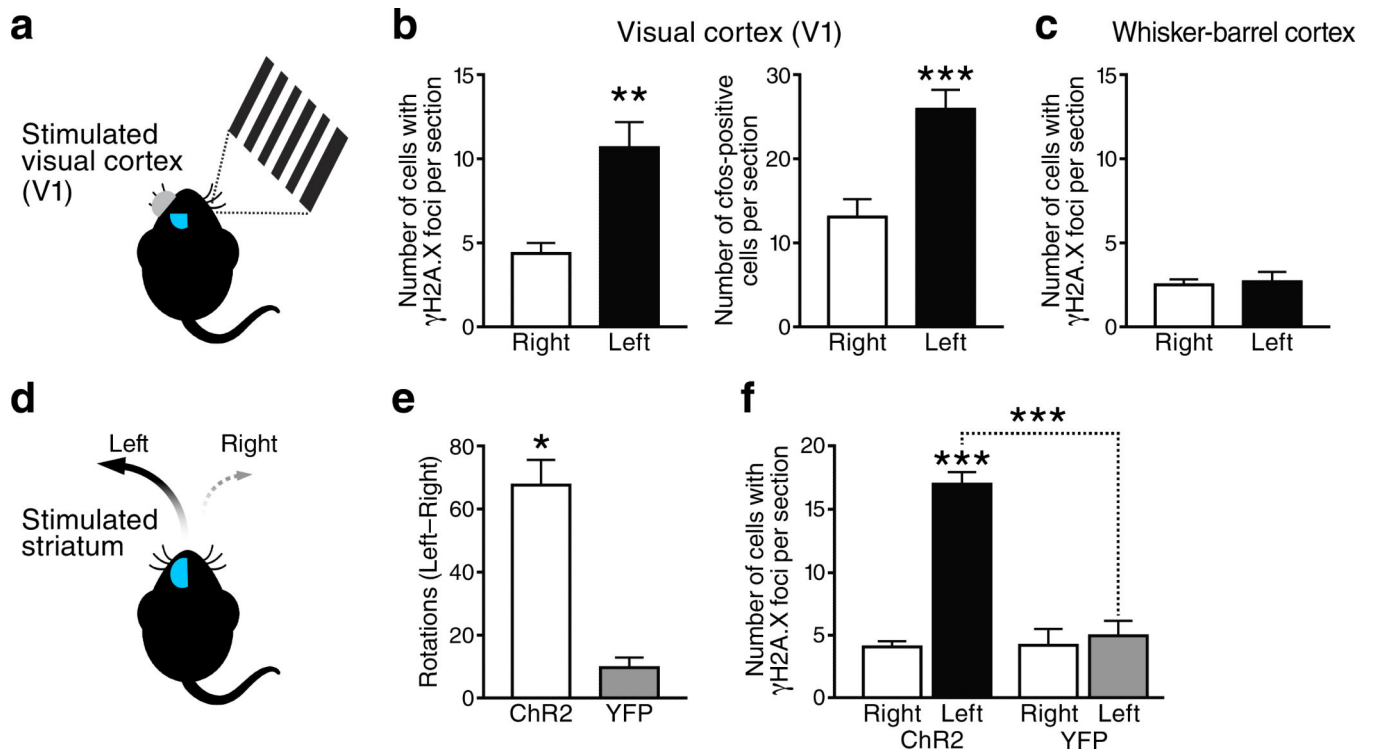


**Figure 4. Network-specific modulation of DSBs by stimulation of primary visual cortex or striatal indirect-pathway neurons**

(a–c) Modulation of DSBs by unilateral visual stimulation of 4-month-old anesthetized mice (n=6). (a) Schematic representation of the experimental design (see Methods for details). Only the right eye was stimulated, whereas the left eye was shielded from light. (b) Numbers of cells with  $\gamma$ H2A.X-positive foci (left) and of c-Fos-positive cells (right) in the primary visual cortex (V1). (c) Numbers of cells with  $\gamma$ H2A.X-positive foci in the whisker-barrel cortex of the same mice. (d–f) Modulation of DSBs and motor behavior by unilateral optogenetic stimulation of the striatum in awake-behaving mice. (d) Schematic representation of the experimental design. Two-month-old mice expressing channel-2-rhodopsin-YFP (Ch2R) in indirect pathway neurons were compared to age-matched mice expressing YFP alone (YFP) (n=3–6 mice per group). The turning behavior of mice was recorded after stimulation of the left striatum. (e) Difference between the numbers of times mice turned left versus right in one hour. Indirect-pathway stimulation induced ipsilateral rotations. The slight trend of YFP mice to turn more left than right was not significant by one-sample t-test. (f) Numbers of cells with  $\gamma$ H2A.X-positive foci in the right and left striatum. \* $p < 0.05$ , \*\* $p < 0.01$ , \*\*\* $p < 0.001$  by two-tailed paired Student's t-test (b, c and e) or vs. leftmost bar and as indicated by brackets (Tukey-Kramer test). Bars represent means  $\pm$  SEM.

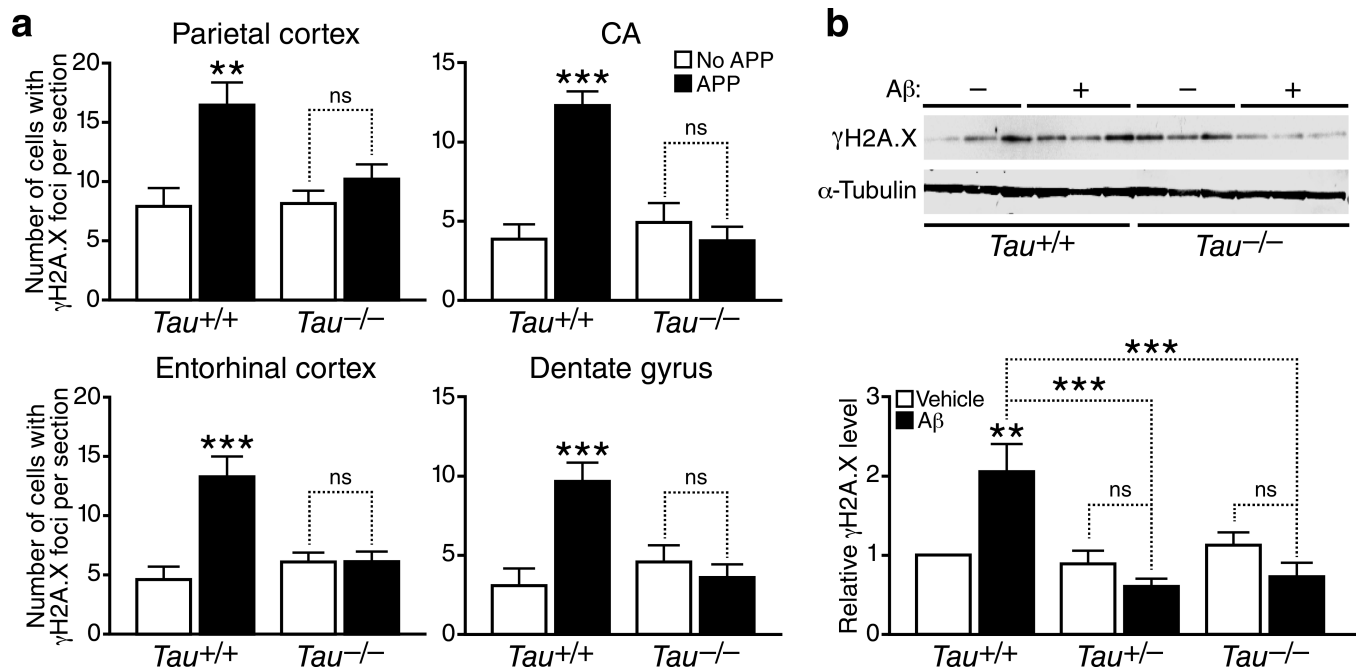


**Figure 5. Tau reduction prevents the A $\beta$ -induced increase in neuronal  $\gamma$ H2A.X foci**  
**(a)** Numbers of cells with  $\gamma$ H2A.X-positive foci per section in different brain regions of 4-month-old *Tau*<sup>+/+</sup> and *Tau*<sup>-/-</sup> mice with or without hAPP expression (n=5–9 mice/genotype). **(b)** Primary forebrain neurons cultured for 15 days *in vitro* (DIV 15) from mice of the indicated *Tau* genotypes were treated with A $\beta$  oligomers (1  $\mu$ M)(+) or vehicle (-) and  $\gamma$ H2A.X levels were determined by western blot analysis. Representative western blots show results from five culture wells and two genotypes (*Tau*<sup>+/+</sup> and *Tau*<sup>-/-</sup>). Quantifications of western blot signals below were from 30 culture wells and three genotypes (*Tau*<sup>+/+</sup>, *Tau*<sup>+/-</sup> and *Tau*<sup>-/-</sup>). n=5 wells per condition from 3 independent experiments. \*\*p<0.01, \*\*\*p<0.001 vs. leftmost bar or as indicated by brackets (Bonferroni *post-hoc* test). n.s., not significant. Bars represent means  $\pm$  SEM.

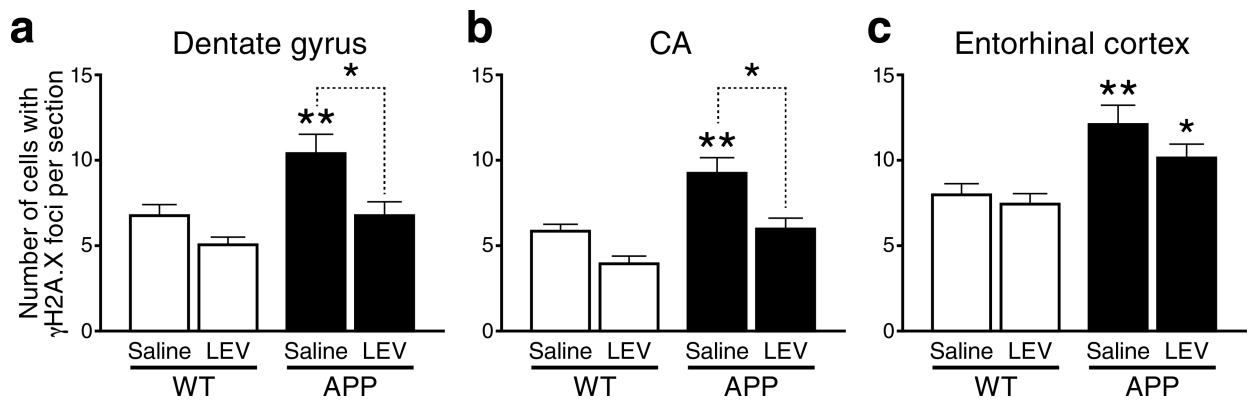


**Figure 6. Levetiracetam normalizes the number of  $\gamma$ H2A.X foci in the hippocampus of hAPP mice**

(a–c) Four- to five-month-old hAPP mice ( $n=5-8$  per treatment) and wildtype controls ( $n=5-6$  per treatment) were treated for 28 days with saline or levetiracetam (75 mg/kg/day by subcutaneous Alzet minipump). The numbers of cells with  $\gamma$ H2A.X-positive foci per section were then determined by immunohistochemistry. \* $p<0.05$ , \*\* $p<0.01$  vs. wildtype or as indicated by brackets (Bonferroni *post-hoc* test). Two-way ANOVA revealed effects of treatment and genotype ( $p<0.01$ ). No significant interaction was observed between them in the hippocampus, and an effect of genotype only ( $p=0.0002$ ) in entorhinal cortex.

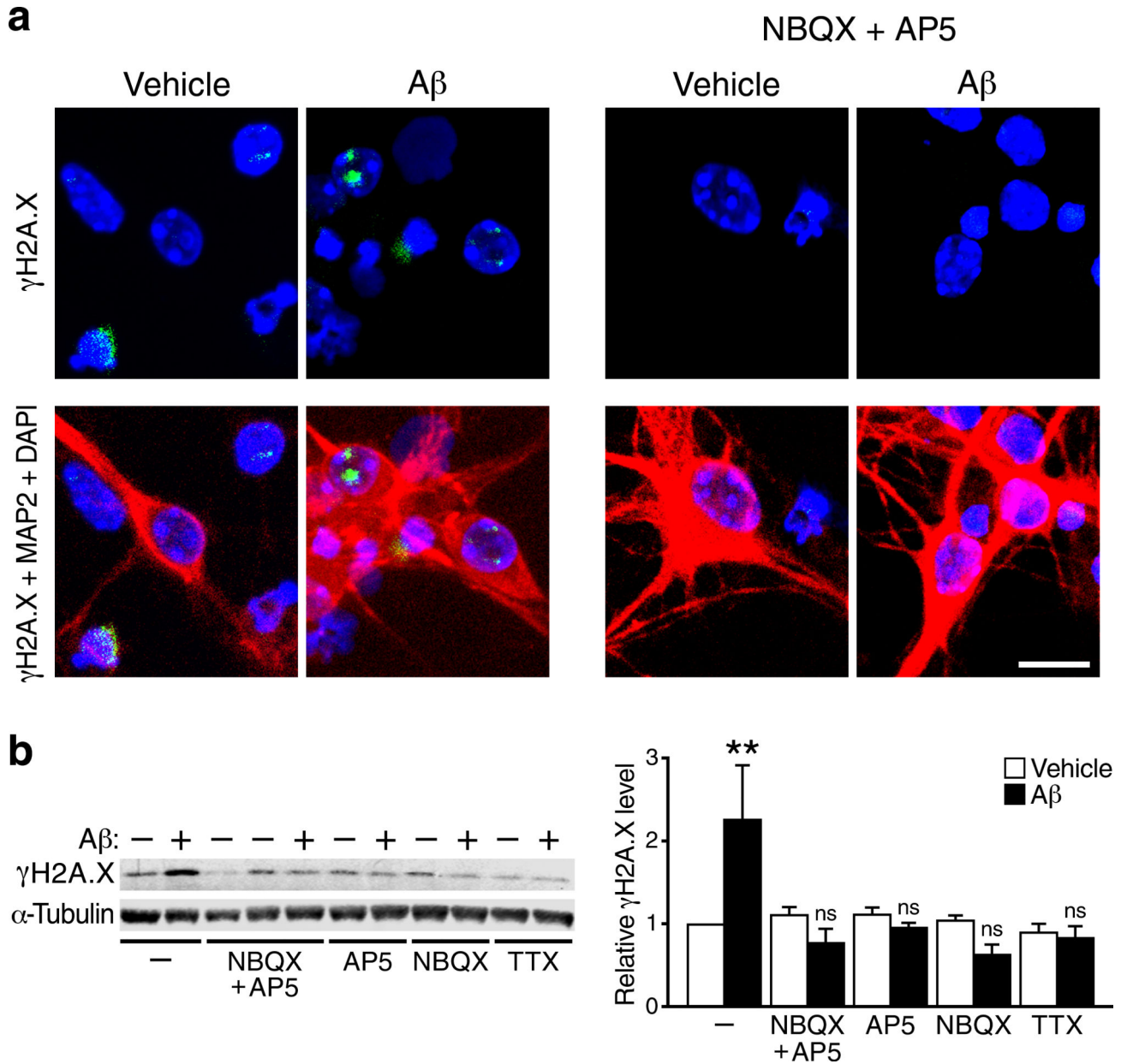


**Figure 7. A $\beta$ -induced increases in  $\gamma$ H2A.X in neuronal cultures depend on neuronal activity**  
**(a)** Primary cultures of wildtype mouse hippocampal neurons (15 DIV) were treated with A $\beta$  oligomers (1  $\mu$ M) or vehicle for 4 hours in the presence or absence of antagonists of AMPARs (NBQX) or NMDARs (APV) as indicated. Cultures were then triple-labeled for  $\gamma$ H2A.X-positive foci (green), the neuronal marker MAP2 (red) and the nuclear marker DAPI (blue). Scale bar: 10  $\mu$ m. **(b)** Primary cultures of wildtype mouse forebrain neurons were treated with A $\beta$  oligomers (1  $\mu$ M)(+) or vehicle (-) for 4 hours in the presence or absence of NBQX, APV, or the sodium channel blocker tetrodotoxin (TTX).  $\gamma$ H2A.X levels were then determined by western blot analysis. A representative western blot is shown on the left and quantifications of western blot signals on the right. n=5–7 wells per condition

from 5 independent experiments. \*\* $p < 0.01$  vs. leftmost bar (Tukey's *post-hoc* test). Bars represent means  $\pm$  SEM.

Author Manuscript

Author Manuscript

Author Manuscript

Author Manuscript

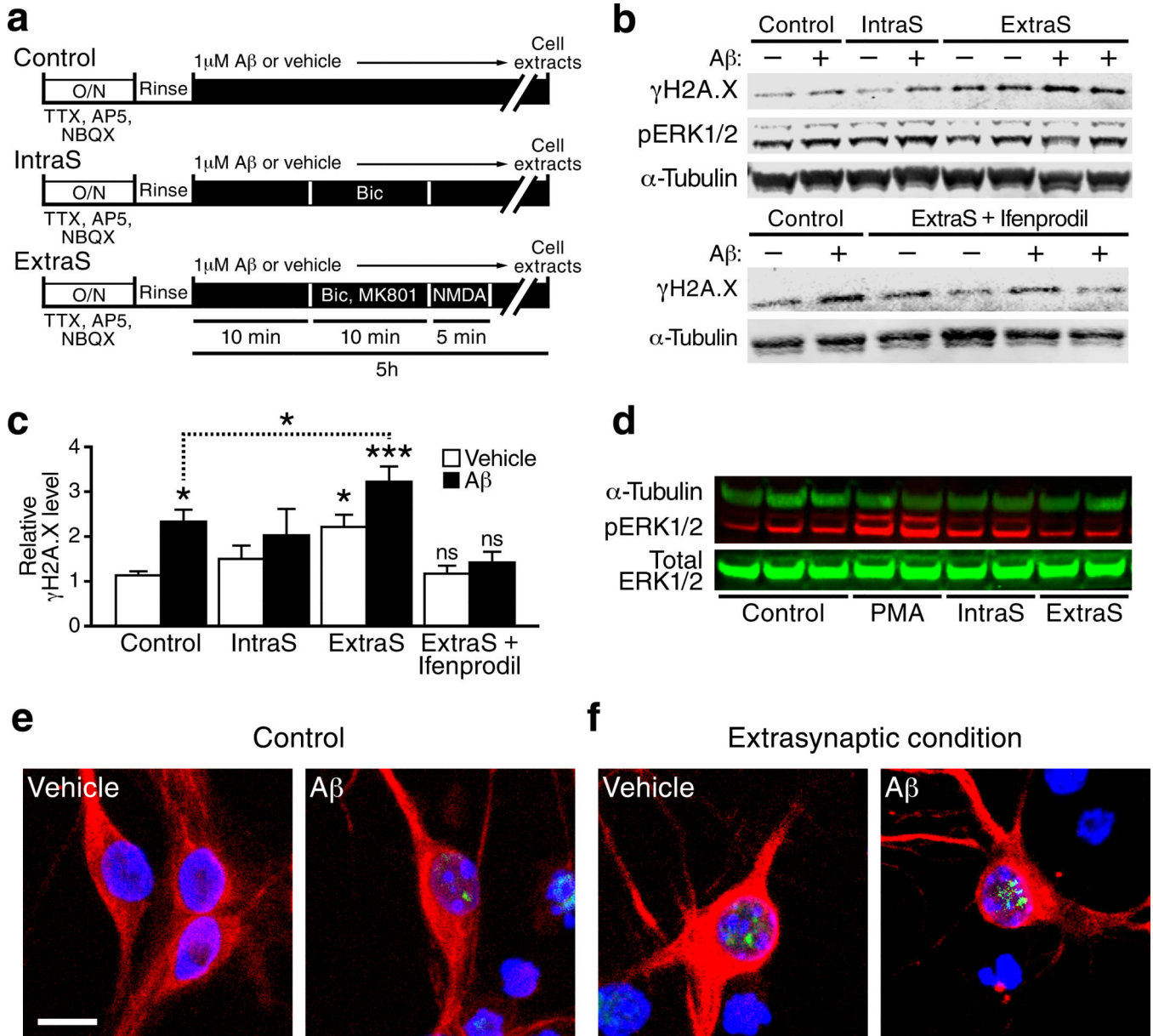


**Figure 8. A $\beta$ -induced increases in  $\gamma$ H2A.X-positive foci in primary neuronal cultures require activation of extrasynaptic NR2B-containing NMDARs**  
**(a)** Wildtype mouse hippocampal neuronal cultures were treated as summarized in the diagram (see Methods for details). Bic, bicuculline. ExtraS, extrasynaptic. IntraS, intrasynaptic. O/N, overnight. **(b, c)** Levels of pERK1/2 **(b)** and  $\gamma$ H2A.X **(b, c)** in primary neurons treated as indicated were determined by western blot analysis. Representative western blots are shown in **(b)** and quantifications of  $\gamma$ H2A.X signals in **(c)**. n=5–12 wells per condition from 7 independent experiments. \*p<0.05, \*\*\*p<0.001 vs. first bar (Dunnett's test) or as indicated by the brackets (two-tailed t-test). Bars represent means  $\pm$  SEM. **(d)** Representative western blot showing the effects of the different treatments on phosphorylation of ERK1/2 (pERK1/2) 30 min after stimulation of cells in the absence of A $\beta$ . PMA, a phorbol ester that activates PKA, leading to ERK1/2 phosphorylation, was used

as a positive control. Compared with the control condition, pERK1/2 levels were higher under conditions favoring spontaneous activation of intrasynaptic NMDARs and lower under conditions favoring activation of extrasynaptic NMDARs. **(e,f)** Primary cultures of wildtype mouse hippocampal neurons plated at low density were treated with A $\beta$  oligomers (1  $\mu$ M) or vehicle for 4 hours under control conditions **(e)** or conditions favoring the activation of extrasynaptic NMDARs **(f)**. Cells triple-labeled for  $\gamma$ H2A.X (green), DAPI (blue) and MAP2 (red) to illustrate their neuronal morphology were visualized by immunostaining and confocal microscopy. Scale bars: 10  $\mu$ m.